A nonlinear filter-bank model of the guinea-pig cochlear nerve: Rate responses

Christian J. Sumner[a) and Lowel P. O'Mard
*Centre for the Neural Basis of Hearing at Essex, Department of Psychology, University of Essex,
Colchester CO4 3SQ, United Kingdom*

Enrique A. Lopez-Poveda
*Centro Regional de Investigación Biomédica, Facultad de Medicina, Universidad de Castilla-La Mancha,
Campus Universitario, 02071 Albacete, Spain*

Ray Meddis
*Centre for the Neural Basis of Hearing at Essex, Department of Psychology, University of Essex,
Colchester CO4 3SQ, United Kingdom*

The aim of this study is to produce a functional model of the auditory nerve (AN) response of the guinea-pig that reproduces a wide range of important responses to auditory stimulation. The model is intended for use as an input to larger scale models of auditory processing in the brain-stem. A dual-resonance nonlinear filter architecture is used to reproduce the mechanical tuning of the cochlea. Transduction to the activity on the AN is accomplished with a recently proposed model of the inner-hair-cell. Together, these models have been shown to be able to reproduce the response of high-, medium-, and low-spontaneous rate fibers from the guinea-pig AN at high best frequencies (BFs). In this study we generate parameters that allow us to fit the AN model to data from a wide range of BFs. By varying the characteristics of the mechanical filtering as a function of the BF it was possible to reproduce the BF dependence of frequency-threshold tuning curves, AN rate-intensity functions at and away from BF, compression of the basilar membrane at BF as inferred from AN responses, and AN iso-intensity functions. The model is a convenient computational tool for the simulation of the range of nonlinear tuning and rate-responses found across the length of the guinea-pig cochlear nerve. © *2003 Acoustical Society of America.* [DOI: 10.1121/1.1568946]

PACS numbers: 43.64.Bt, 43.66.Ba [LHC]

I. INTRODUCTION

Models of signal processing in the auditory periphery are important tools for advancing our understanding of hearing. For example, in psychophysics, models of the cochlea are important components in theories of the perception of pitch (Meddis and Hewitt, 1991a, b; Patterson *et al.*, 1995; Pressnitzer *et al.*, 2002), the segregation of concurrent vowels (Assman and Summerfield, 1990; Meddis and Hewitt, 1992), and binaural precedence (Hartung and Trahiotis, 2001). Computational models of auditory scene analysis also include auditory peripheral models as front-ends (Brown and Cooke, 1994; Ellis, 1996). In audio engineering applications, compression algorithms employ models of psychophysical masking, to decide which parts of a signal can be safely removed (e.g., Brandenburg, 1996; Brandenburg and Bosi, 1997). Speech recognition systems also benefit from employing auditory models, as front-ends in noisy environments (e.g., Ghitza, 1988; Hermansky, 1998; Tchorz and Kollmeier, 1999).

In physiology, computational models of the AN are a useful tool for investigating cochlear processing itself. Some models, like the one here, attempt to reproduce complete peripheral responses (Deng and Geisler, 1987; Jenison *et al.*, 1991; Carney, 1993; Giguere and Woodland, 1994; Robert and Eriksson, 1999; Zhang *et al.*, 2001). Such models integrate facts and theories from a wide range of research in the cochlea. They allow the investigation of speech coding in the auditory periphery (e.g., Deng and Geisler, 1987; Jenison *et al.*, 1991) without the need for animal experimentation. A suitably flexible model, such as presented here, can also be used to simulate cochlear pathology (e.g., Schoonhoven *et al.*, 1994; Giguere and Smoorenburg, 1998; Lopez-Poveda and Meddis, 2001b) and the responses to noise trauma (Sachs *et al.*, 2002), and thus has the potential to inform hearing aid development. Peripheral models are also an essential prerequisite for the modeling of *in vivo* responses in the brain-stem (e.g., Hewitt and Meddis, 1992).

Tuning in the cochlea is nonlinear (Rhode, 1971). However, the mechanical filtering of the cochlea has traditionally been modeled as a bank of parallel linear band-pass filters (Patterson *et al.*, 1988). Recently, there have been several attempts to extend computational models to capture the known nonlinear effects (Jenison *et al.*, 1991; Robert and Erikson, 1999; Zhang *et al.*, 2001; Goldstein, 1990, 1995; Irino and Patterson, 2001).

Meddis *et al.* (2001) have also described an architecture for modeling nonlinear mechanical filtering: the dual resonance nonlinear (DRNL) filter. The DRNL filter has been

---

[a)Author to whom correspondence should be addressed. Current address: Kresge Hearing Research Institute, University of Michigan, Ann Arbor, MI 48109-0506. Electronic mail: cjsumner@umich.edu

shown, by use of different parameter sets, to reproduce the different tuning and nonlinear basilar membrane (BM) input–output (I/O) functions at different locations along the cochlea. It also reproduces variations in phase response with frequency and level, two-tone suppression, local distortion products, and impulse responses on the BM. Using this filter architecture, Lopez-Poveda and Meddis (2001a) modeled human psychophysical measures of tuning and compression at different BFs.

Cochlea nonlinearities can also be measured at the level of the AN (Yates *et al.*, 1990; Sachs and Abbas, 1974) where they affect the shape of rate-intensity (RI) functions. In the guinea-pig, there are three types of RI function: (a) "saturating:" having high SR, low thresholds, steep RI functions and small (~20 dB) dynamic ranges; (b) "sloping saturation" which have less spontaneous activity, higher thresholds, and do not saturate completely, but show a sloping-saturation; and (c) "straight" which have little or no SR, high thresholds and no steep part in their RI function, just a long slope (Winter *et al.*, 1990). Sumner *et al.* (2002) recently described a thorough revision to the Meddis (1986, 1988) inner-hair-cell (IHC) model. When used with a DRNL filter, this model has been shown to reproduce accurately much of the variety of responses seen in the guinea-pig IHC and AN at high best frequencies (BFs; ~18 kHz). This includes the variation of rate-intensity functions for different fiber types, variation with stimulus frequency, the fall off of phase locking with stimulus frequency, adaptation (Sumner *et al.*, 2003), and the stochastic release of neurotransmitter.

We will describe the integration of the DRNL model of mechanical filtering (Meddis *et al.*, 2001) and the new model of inner-hair-cell transduction (Sumner *et al.*, 2002) to produce a complete filterbank model of the guinea-pig cochlea. Previous studies (Meddis *et al.*, 2001; Sumner *et al.*, 2002, 2003) did not place the filters within a filterbank framework, but instead changed parameters individually at different best frequencies. This model seeks to reproduce AN responses at all BFs, using parameters that change smoothly along the full length of the cochlea. Meddis *et al.* (2001) reproduced the responses of the BM at three BFs, 800 Hz, 9 kHz, and 18 kHz. This leaves a considerable gap at frequencies vital for understanding auditory processing of speech and music. Below 5 kHz, there are considerable changes in tuning and compression with BF. The BM data were also taken from more than one species. Furthermore, it is well known that such preparations are physiologically very vulnerable. This limits the collection of the data, and the measurements may not reflect the intact cochlea accurately. Here we have used AN data, which is less invasive, comes from a wide range of BFs including those relevant to speech, and is from a single species.

We will focus here on four different aspects of the responses to single tones: threshold tuning curves; BM compression as measured from AN responses; variation of tuning with level; and RI functions from different types of fibers and the relationship between SR and threshold. For all these, we are especially concerned to accurately represent the changes along the length of the cochlear partition. We intend the model, which is publicly available as part of an extensive

suite of auditory modeling tools,[1] for use both as an input to larger scale models of auditory processing in the brain-stem and beyond, and as a predictor of AN responses. It may additionally help to refine of our understanding of signal processing in the cochlea.

II. THE MODEL

A. Middle-ear filtering

The response of the middle ear is modeled by a cascade of two linear band-pass Butterworth filters. This replaces the single band-pass filter used previously (Sumner *et al.*, 2002, 2003). The change was necessary to reproduce the thresholds found by Evans (1972). One filter is second order with an upper cutoff of 25 kHz and a lower cutoff of 4 kHz. The other filter is third order with upper and lower cutoffs of 30 kHz and 700 Hz. Both have unity gain in the passband. The input to the filter is sound pressure (μPa). This is scaled by a factor of 1.4×10^{-10} so that the filter outputs, $x(t)$, reflect measured stapes velocities (Nuttall and Dolan, 1996) in ms^{-1}. Additionally, a variable gain, G_{me}, is introduced at this stage. This is necessary to reproduce overall sensitivity differences between different preparations. G_{me} is 0 dB unless stated.

B. Mechanical filtering: DRNL filter

The filtering of the BM is modeled with a "dual-resonance-non-linear" (DRNL) filter architecture that has been described and evaluated more fully elsewhere (Meddis *et al.*, 2001). Only the parameter values vary from the model that was presented previously. Figure 1 shows the architecture. It consists of two parallel pathways, one linear (upper pathway in Fig. 1) and the other nonlinear (lower pathway), whose outputs are summed to produce the filter output, $v(t)$. The compression in the nonlinear pathway is described by

$$y[t] = \mathrm{SIGN}(x[t]) \times \mathrm{MIN}(a|x[t]|, b|x[t]|^{\nu}), \qquad (1)$$

where a, b and v are parameters determining the exact behavior.

Meddis *et al.* (2001) showed that the model could be fit to BM laser-interferometry data for three different BFs, by varying the DRNL filter parameters. Figures 2(a) and (b) show the effects of the parameters. At high-BFs the nonlinear pathway has a higher center frequency ($CF_{lin} < CF_{NL}$), narrower bandwidth ($BW_{NL} < BW_{lin}$) and higher gain ($a > G_{lin}$) than the linear path. The result at threshold is a narrowly tuned filter, with a wide-bandwidth low-frequency tail. Also, the response at CF_{NL} is compressed over a large dynamic range. At low BFs the two pathways are very close in center-frequency ($CF_{lin} \sim CL_{NL}$) and gain ($a \sim G_{lin}$). The nonlinear pathway dominates the BF response only at low levels. At high levels the linear pathway dominates the BF response, and at intermediate levels the output is a mix of the two. Thus the variation in measured compression with BF can emerge without any change in the compression exponent v.

To implement the filterbank, we adopted the scheme of Lopez-Poveda and Meddis (2001a). The values of the parameters a, b, the bandwidths of both pathways (BW_{lin} and
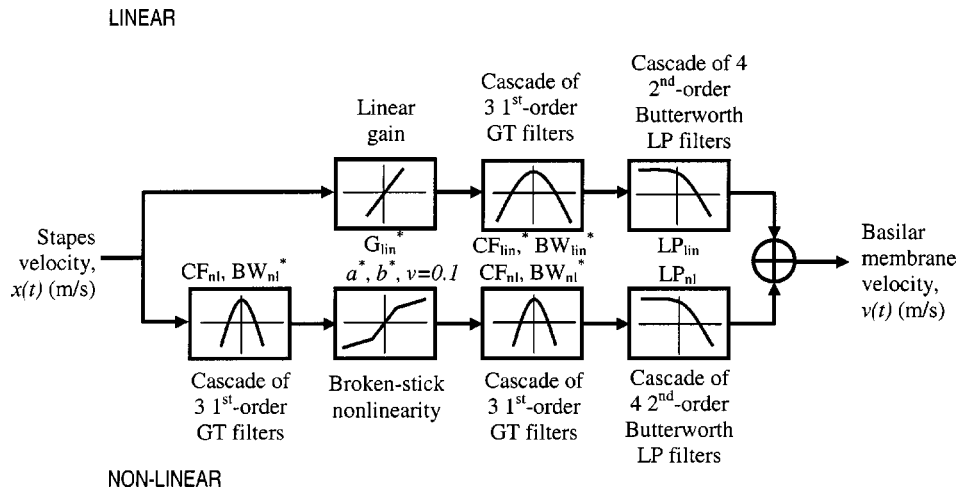
LINEAR

Linear
gain

Cascade of
3 1st-order
GT filters

Cascade of 4
2nd-order
Butterworth
LP filters

Stapes
velocity,
$x(t)$ (m/s)

CF_{nl}, BW_{nl}^*

G_{lin}^*
a^*, b^*, $v=0.1$

CF_{lin}^*, BW_{lin}^*
CF_{nl}, BW_{nl}^*

LP_{lin}
LP_{nl}

Basilar
membrane
velocity,
$v(t)$ (m/s)

Cascade of
3 1st-order
GT filters

Broken-stick
nonlinearity

Cascade of
3 1st-order
GT filters

Cascade of
4 2nd-order
Butterworth
LP filters

NON-LINEAR

FIG. 1. Schematic of the DRNL filter architecture. The filter output is a sum of a linear and a nonlinear pathway. The linear (upper) pathway is a gain followed by a gammatone filter (GT; Patterson *et al.*, 1988) and a low-pass (LP) filter. The nonlinear (lower) pathway consists of the following cascade; a gammatone filter, a compression function, a second gammatone filter, and a low-pass filter. Parameters which are allowed to vary with BF are indicated with an asterisk (*). Bandpass center frequencies and low-pass filter cutoffs are of the same frequency within a single pathway, i.e., $LP_{NL}=CF_{NL}$ and $LP_{lin}=CF_{lin}$. All filters have unity gain in the pass-band. CF_{NL} is always set to the specified BF of the filter.

BW_{NL}), the gain of the linear filter (G_{lin}), and the center frequency of the linear filter (CF_{lin}) were made to vary linearly on a log-log scale as a function of best frequency (BF):

$$\log(\text{parameter}) = p_0 + m \log(CF), \qquad (2)$$

where p_0 determines the parameter values at a theoretical BF of 1Hz, and m determines the slope of the parameter with BF on a log-log scale. All the parameter values are given in Table I. The parameters that vary with BF are also indicated with an asterisk (*) in Fig. 1. The remaining parameters, which are order of the filter cascades and the compression exponent, were fixed across the entire filter bank. These values are given explicitly in Fig. 1 as well as Table I. The nonlinear pathway center frequency (CF_{NL}) is set equal to BF.

C. Transduction: IHC

The IHC transduction model has been described in detail by Sumner *et al.* (2002, 2003). The first stage is a simple biophysical model of the cilia transduction and receptor potential (RP) response (modified from Shamma *et al.*, 1986). The second stage of transduction simulates the presynaptic calcium processes that lead to the release of neurotransmitter. Two parameters at this stage determine the fiber type. The third IHC stage models the manufacture, release, loss, and reuptake of neurotransmitter vesicles at the synapse. This is a quantal version of the model of adaptation proposed by Meddis (1986). The refractory stage then imposes an absolute and relative refractory period, reducing the probability that a vesicle will trigger an action potential.

Sumner *et al.* described how the model AN fiber response depends on the choice of the two calcium parameters: G_{Ca}^{max}, the maximum calcium conductance in the vicinity of the synapse, and $[Ca^{2+}]_{thr}$, the threshold concentration of calcium required for release. The effects of the parameters are shown in Fig. 2(c). In terms of gross characteristics, a large value of G_{Ca}^{max} ($\sim 6-7$ nS) will result in a fiber with high-spontaneous-rate (HSR) type characteristics, while a

small value ($\sim 1-3$ nS) produces a low-spontaneous-rate (LSR) fiber. The continuous lines in Fig. 2(c) show this. $[Ca^{2+}]_{thr}$ affects primarily the low intensity responses, and thus affects the spontaneous rate (SR) and threshold of the unit. The dotted lines in Fig. 2(c) show this. An additional parameter, M, in the synapse, scales the vesicle release rate linearly. It is varied to determine the overall firing rate of model fiber responses. The effect of M on RI functions is shown fully in Sumner *et al.* (2002).

The relationship between the parameters and the spontaneous rate can be described analytically:

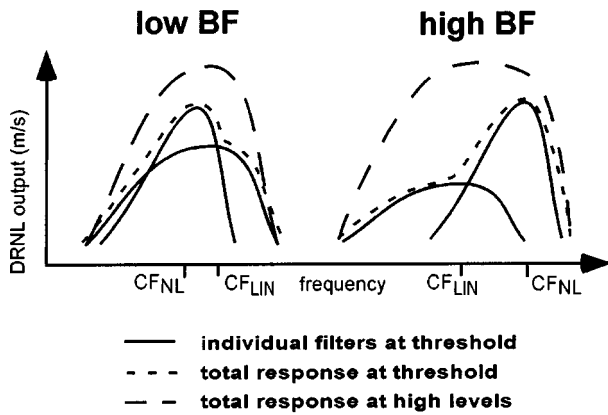$$SR = \frac{10 M k_{SR}}{10 + 0.28 k_{SR}}, \qquad (3)$$

where

$$k_{SR} = \max(\lfloor 4.65 \times 10^{25}(G_{Ca}^{max})^3 - 20 \times 10^{31}([Ca^{2+}]_{thr})^3 \rfloor, 0).$$

The relation of threshold with spontaneous rate is examined in Sec. III D.
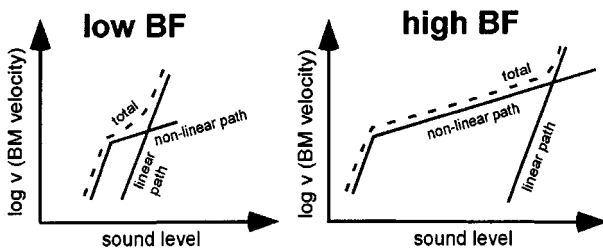
D. Model implementation and development

The development of model parameters started with those of previous studies. The initial DRNL filterbank parameters were taken from Lopez-Poveda and Meddis (2001b). The compression exponent, v, was changed from 0.25 to 0.1 dB/dB across all BFs, to reflect the compression estimated by Cooper and Yates (1994) and Yates *et al.* (1990) in the guinea-pig. The DRNL filter parameters were refined progressively from the starting values. For each BF, we looked for a single set of parameters to fit the frequency-threshold tuning curves of Evans (1972) and the RI functions of Cooper and Yates (1994). We then fitted Eq. (2) to these parameter values and reevaluated the complete filterbank. Following previous studies, the orders of the filters were the same for all BFs, but as global parameters they were allowed to vary. The model was fitted by hand. The goal was to arrive at a single set of parameters that gave a good compromise be-

A. Variation in DRNL tuning

low BF **high BF**

DRNL output (m/s)

CF$_{NL}$ CF$_{LIN}$ frequency CF$_{LIN}$ CF$_{NL}$

—— individual filters at threshold
- - - total response at threshold
— — total response at high levels

B. Variation in DRNL IO functions

low BF **high BF**

log v (BM velocity)

total
non-linear path
linear path

sound level

log v (BM velocity)

total
non-linear path
linear path

sound level

C. Effect of synapse parameters on RI functions

spike rate

M

G_{Ca}^{max}

$[Ca^{2+}]^{thr}$

sound level
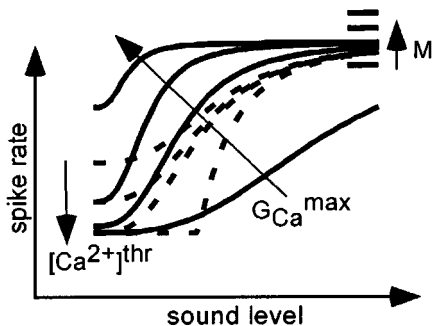
FIG. 2. How model parameters determine the response characteristics. (a) The variation in DRNL filter tuning with level and BF. Continuous lines show the frequency response of the linear and nonlinear pathways at threshold. CF$_{NL}$ and CF$_{lin}$ indicate the center frequencies of the nonlinear and linear paths, respectively. The dotted lines show the combined response at threshold, and the dashed lines show the response at high stimulus levels. (b) Variation in the DRNL filter IO function with BF in response to stimulation at BF. Continuous lines indicate the responses of the linear and non-linear pathways. Dotted lines indicate the combined DRNL filter output. (c) Effect of varying synapse parameters G_{Ca}^{max} (continuous lines), $[Ca^{2+}]_{thr}$ (dotted lines) and M. For all panels, arrows show the direction of function change for an increase in each parameter value. M scales the response rate linearly across the entire dynamic range [see Eq. (3) and also Sumner *et al.* (2002)].

tween the different data sets. The filterbank was further tuned in light of the result of evaluation against four AN fiber iso-intensity response maps at three different BFs. Two of the fibers were collected by Winter and Robertson (personal communication) at our request. The other two AN fiber responses were taken from Müller and Robertson (1991). The final set of parameters found is given in Table I.

The initial IHC parameters were taken from Sumner *et al.* (2002). However, the parameters that determine fiber type were varied (see Sec. II C). For simulations involving the whole filterbank, the IHC parameters were fixed across all BF, creating generic high-, medium-, and low-spontaneous rate responses. The values are given in Table I. For the fitting of frequency threshold tuning curves, the IHC parameters were fixed at the values given for the generic HSR fiber in Table I. For the fitting of rate-intensity and iso-intensity functions, these parameters were allowed to vary from fiber to fiber. Additionally, the middle-ear-gain parameter, G_{me}, was varied between data from different animals. This was found to be necessary to model differences in overall response with level. Fitting of these parameters was done by hand, guided by the principles shown in Sec. II C and Fig. 2(c). Parameters for individual fibers are given in the figure legends.

Frequency tuning curves (FTCs) were generated using a two-down–one-up-tracking procedure, as described by Relkin and Pelli (1987). RI functions were generated using 100-ms tone pips with 2.5-ms linear ramps. They were presented at a range of sound levels, and often at a range of stimulus frequencies. For each stimulus condition, the stochastic stages of the model were run 20 times to produce a reliable measure of firing rate. Firing rate was calculated over the full period of stimulus presentation.

Cooper and Yates (1994) have inferred BM IO functions at BF from animal AN fibers using a technique described by Yates *et al.* (1990). We have applied their methods to the RI functions produced by the model, in so far as was practical. For each point on the BF RI function, we calculate the sound level required for an off-BF tone to produce the same firing rate. Plotting the off-BF sound level versus BF sound level for a given firing rate yields the BM IO function. The exact off-BF level was calculated by linearly interpolating between the two adjacent off-BF sound levels. Average slopes of model IO functions were calculated by the fitting of a straight line using least squares regression. When the gradient of the function above and below the threshold for compression were clearly different, the fitting of the line was restricted to the high-level portion above any abrupt change in slope associated with the compression threshold.

All the model code has been implemented in C, and is available publicly as source code.[1] MATLAB was used as a harness for control of executables, manipulation of parameters, and analysis of output.

III. EVALUATION OF THE MODEL

A. Filter tuning characteristics at threshold

The tuning characteristics of the AN at threshold are typically described by a frequency-threshold-curve (FTC).

TABLE I. Model parameters.

DRNL filter parameters that are fixed across all BFs	
Compression exponent, ν (dB/dB)	0.1
Gammatone cascade of nonlinear path	3
Low-pass filter cascade of nonlinear path	4
Center frequency of nonlinear path, CF_{NL}	Set equal to BF
Low-pass cutoff of nonlinear path, LP_{NL}	Set equal to BF
Gammatone cascade of linear path	3
Low-pass filter cascade of linear path	4
Low-pass cutoff of linear path, LP_{lin}	Set equal to CF_{lin}

DRNL filter parameters that vary with BF: $p(BF) = 10^{p_0 + m \log_{10}(BF)}$	Filter-bank coefficients		Single filter at 6 kHz BF [in Fig. 5(b)]. Filterbank values shown in brackets.
	p_0	m	
Bandwidth of nonlinear path, BW_{NL} (Hz)	0.8	0.58	980 (unchanged)
Compression parameter, a	1.87	0.45	251 (3716)
Compression parameter, b	−5.65	0.875	4.52×10^{-3} (unchanged)
Center frequency of linear path, CF_{lin} (Hz)	0.339	0.895	2961 (5253)
Bandwidth of linear path, BW_{lin} (Hz)	1.3	0.53	634 (2006)
Linear path gain, G_{lin}	5.68	−0.97	103 (unchanged)

IHC parameters	HSR	MSR	LSR
$[Ca^{2+}]^{thr}$ threshold Ca^{2+} conductance	0	3.35×10^{-14}	1.4×10^{-11}
M, max. free transmitter quanta	10	10	10
G_{Ca}^{max}, max. Ca^{2+} conductance (nS)	7.2	2.4	1.6

Figure 3(a) shows the FTCs for a selection of guinea-pig AN fibers (Evans, 1972). The tuning clearly shows characteristic tip and tail regions at high BFs. At low BFs the tip is much less prominent, and thresholds are higher. Figure 3(b) shows FTCs generated by the model using the DRNL filterbank. The filterbank parameters were created by applying the coefficients p_0 and m in Table I to Eq. (2). The IHC model used the generic "HSR" parameter set given in Table I. The model FTCs agree reasonably well with the data.

Evans summarized the characteristics of the tips of the tuning curves for a large population of AN fibers. Figure 4 shows the animal data statistics (dots), compared with the behavior of the model (continuous lines). Figure 4(a) shows the filter Q-factor (filter BF divided by bandwidth) for 10 dB above the BF threshold (Q_{10}). This is a measure of the sharpness of tuning. In the data Q_{10} rises with BF, from around 1 at 200 Hz to between 3 and 10 at 10 kHz. Figures 4(b) and (c) show the slopes of the tuning curves above and below the unit BFs, calculated for stimulus frequencies whose thresholds lay within 25 dB of the BF threshold. Overall, the model conforms well to the measured data. There are some discrepancies in the shapes of the FTCs and the agreement with the summary statistics. The fit to FTCs has been compromised in order to fit the RI functions of Cooper and Yates (1994), using the same DRNL filterbank parameter set.

B. Compression characteristics across the cochlear nerve

Yates *et al.* (1990) have proposed a method for deriving BM IO functions from AN fiber measurements. AN rate responses are recorded both at BF and also at a stimulus frequency below BF. Below BF, the IHC is assumed to be driven by a linear BM. Thus any nonlinearities evident in the AN response to a below BF stimulus must be associated with the transduction process. It is also assumed that the frequency of stimulation does not affect the transduction nonlinearity. By equating firing rates for on-and off-BF responses, a putative BM IO function at BF can be derived (see Yates *et al.*, 1990, and also Sec. II D, for more details). A derived IO function is limited to within the dynamic range of the fiber at BF.

Cooper and Yates (1994) derived BM IO functions from AN rate responses across a wide range of BFs in a single animal. Figures 5(a)–(c) show three BM IO slopes that they derived (unconnected squares). At high BFs (6 and 23 kHz), the BM IO function is linear at low levels and highly compressed at high levels (0.1 dB/dB). However, at low BF (1800 Hz), the BM IO function is less compressive and almost straight, with a slope of 0.5 dB/dB. The derived IO slopes of the model (thick continuous lines) using the filterbank parameters given in Table I are shown on the same axes as the data. In Figs. 5(a) and (c) they agree well with the animal data of Cooper and Yates. In Fig. 5(b), at 6 kHz BF, the model IO function retains the same shape as the data below about 80 dB, but is shifted to lower intensities. Above 80 dB the model IO function rises again. This reflects the linear pathway, contributing to the high-level response at BF. The dashed line shows the response of the model for a single DRNL filter that has been modified to fit the data. The parameters which give a good fit to the BF response are in Table I. These are the actual parameter values for a single BF, rather than the values for Eq. (2). The main parameter change is the reduction in a, the gain of the low-intensity linear part of the DRNL filter broken-stick function [see Fig. 2(b)]. This lowers the gain of the tip of the tuning curve,
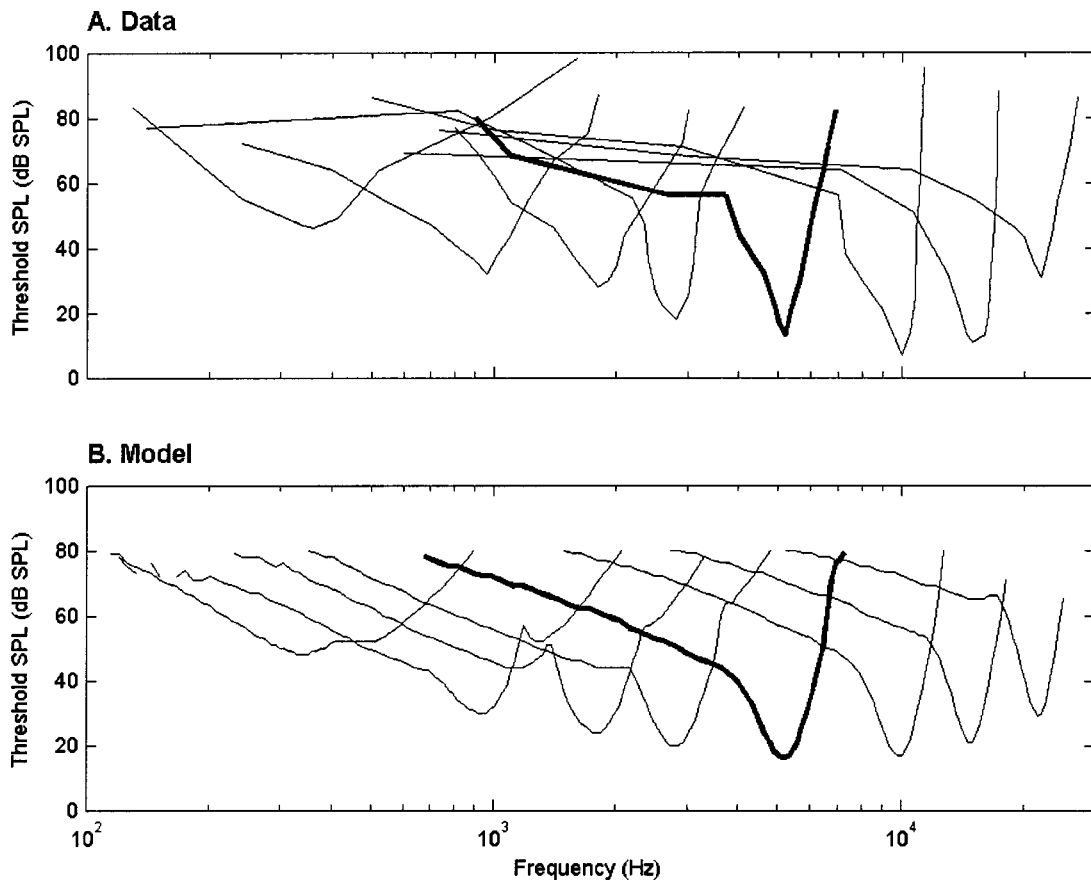
A. Data

B. Model

FIG. 3. Frequency threshold tuning curves (FTCs). (a) Guinea-pig AN (Evans, 1972). (b) Model using filter-bank DRNL filter parameters and "HSR" synapse parameter set (Table I).

raising the level at which the IHC reaches threshold, and the level at which the DRNL filter response becomes compressed. The contribution of the linear pathway at BF has also been reduced to remove the high-level return to linearity.

A more rigorous test of the model than the derivation of BM IO functions was to fit the RI functions from which the IO functions were derived. Figures 5(d)–(f) show this. On each axis two RI functions are plotted from a single guinea-pig fiber: one at BF (open squares) and one somewhat below BF (dots). The continuous lines show the fits of the model to the RI functions using the filterbank parameters of Table I. It

was from these that the continuous lines in Figs. 5(a)–(c) were calculated. A good fit of the data RI functions must lead to a good fit of the data IO functions. The IHC parameters (G_{Ca}^{max}, $[Ca^{2+}]_{thr}$ and M) were allowed to vary between fibers. The parameters used are given in the figure legend. In Fig. 5(e), like Fig. 5(b), the fit of the filterbank at BF is poor. This is because the BF response of the filterbank model is much more sensitive than these data. Note that this is not a failure of the model. There is a clear disparity among the different data sets. In Fig. 5(e) the difference in thresholds between the BF and 2 kHz is about 20 dB. In Fig. 3(a), at a similar BF (marked) the difference between the thresholds
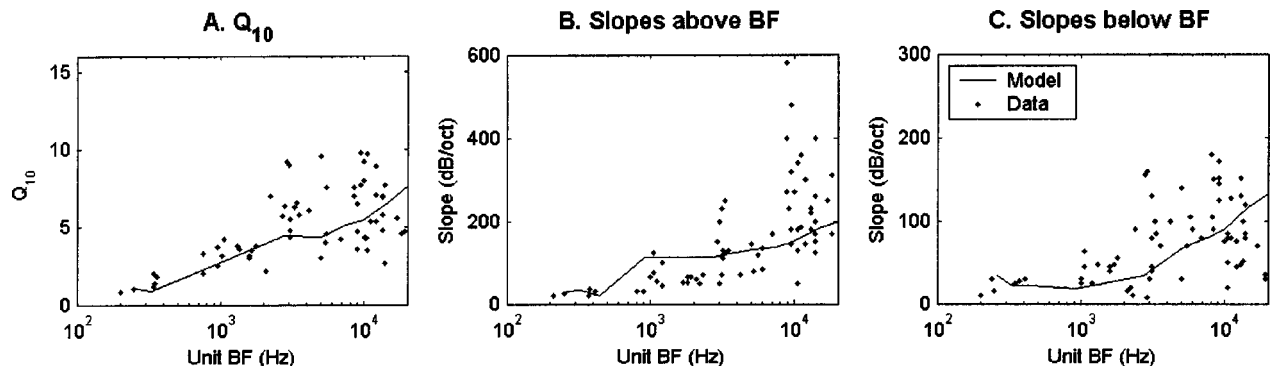

FIG. 4. Summary statistics describing the shapes of the tuning curves. Dots indicate data (Evans, 1972) and continuous lines indicate the behavior of the model. (a) Filter Q_{10} (BF/bandwidth at 10 dB above BF threshold). (b) Slopes of the tuning curves above the unit BF, within 25 dB of BF threshold. (c) Slopes of the tuning curves below the unit BF, within 25 dB of BF threshold.
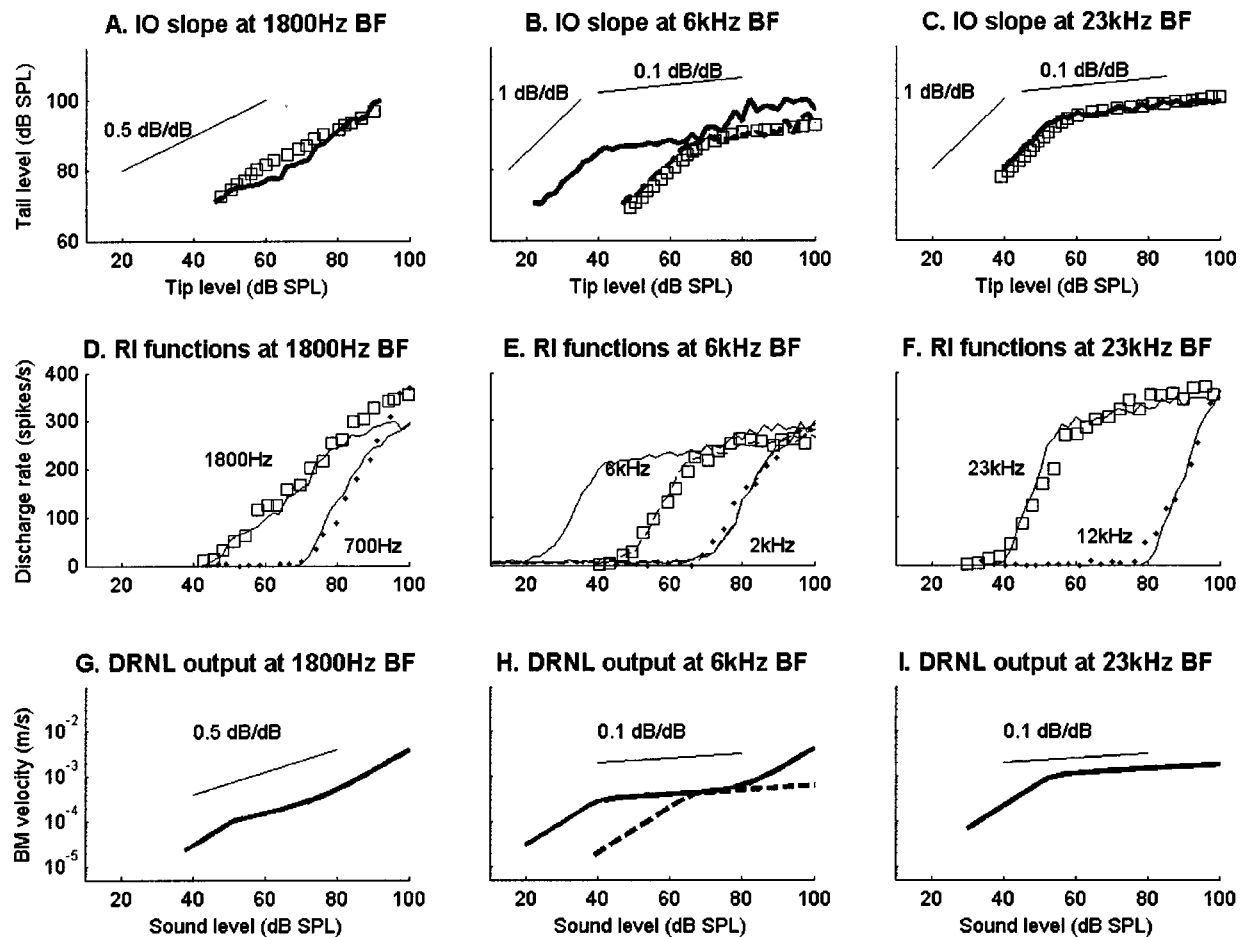
FIG. 5. (a)–(c) IO functions derived from AN responses. Unconnected squares are derived IO functions from Cooper and Yates (1994). Continuous lines are the responses of the model. The dashed line in (b) shows the IO function for the model that fits the RI functions in (e). (d)–(f) The RI functions for the medium spontaneous rate fibers from which the IO functions in (a)–(c) were derived. Unconnected squares are the data points at BF (Cooper and Yates, 1994, Fig. 2, panels A, C and F); unconnected dots are the data below BF; continuous and dashed lines indicate the fits of the model to the data. Model results are generated using the DRNL filter-bank parameters, except the dashed lines in (b) and (e), which use the individual "single filter at 6 kHz BF" DRNL filter parameters given in Table I. Synapse parameters used in (a) and (d): $G_{Ca}^{max}=1.27$ nS, $[Ca^{2+}]_{thr}=3\times10^{-11}$, $M=14$; in (b) and (e): $G_{Ca}^{max}=3$ nS, $[Ca^{2+}]_{thr}=1.4\times10^{-11}$, $M=9$; in (c) and (f): $G_{Ca}^{max}=2.9$ nS, $[Ca^{2+}]_{thr}=2.5\times10^{-11}$, $M=15$. In all cases, $G_{ME}=0$. (g)–(i). The outputs from the DRNL filters in response to BF stimuli, before they are input to the IHC stage. BM velocity is computed as the maximum response during the stimulation period. The continuous lines are for the DRNL filter-bank parameters. The dashed lines in (h) show the response of the "single filter at 6 kHz BF" parameter set in Table I.

for a BF tone and for a 2 kHz tone is about 40 dB. The reduction of a enables us to fit the BF RI function at the same time as the off-BF function in Fig. 5(e) (dashed line).

Figures 5(g)–(i) show the outputs from the DRNL filter at BF. This allows us to compare the real IO function of this stage of the model with the derived IO functions in Figs. 5(a)–(c). At 6- and 23-kHz BFs, the DRNL filter output at BF shows clear regions of linearity and compression which correspond excellently with those of the derived IO functions. In Fig. 5(g), the 1800-Hz BF output from the DRNL filter shows a region of compression between 50 and 80 dB SPL. Within that region the compression is slowly changing. This trend is less obvious in the output from the model AN fiber [Fig. 5(d)]. Stochasticity makes small features harder to see. It is also the case that the derived slopes become less well defined in a statistical sense, near to threshold and close to saturation (see Winter and Palmer, 1991).

The derived high-intensity BM IO slopes of more guinea-pig AN data from Cooper and Yates are shown in Fig. 6 (open squares). Above 5 kHz, derived IO slopes are around 0.1 dB/dB. Below there, there is an increase in the derived

slope, to around 0.5 dB/dB. Figure 6 also shows the derived AN IO slopes for the model (continuous line). RI functions were all generated using the DRNL filterbank parameter set (Table I), and the "LSR" synapse parameter set (Table I). The model shows good agreement with the data.

C. Nonlinear tuning characteristics

The model was tuned to reflect two different data sets that are almost independent measures of threshold tuning and compression. However, the frequency dependence of the derived IO slope affects the variation of tuning with level. Figures 7(a)–(d) show rate responses of four different AN fibers, as iso-intensity contours. Each line shows how firing rate depends on stimulus frequency at a given level. At low BFs [400 Hz, Fig. 7(a); data was provided by Donald Robertson and Ian Winter], the response is broad and almost symmetrical. However, at high sound levels, firing rates are higher at frequencies above BF than below BF. At 3-kHz BF [Fig. 7(b); data provided by Donald Robertson and Ian Winter] the response is almost symmetrical at low levels but the activity
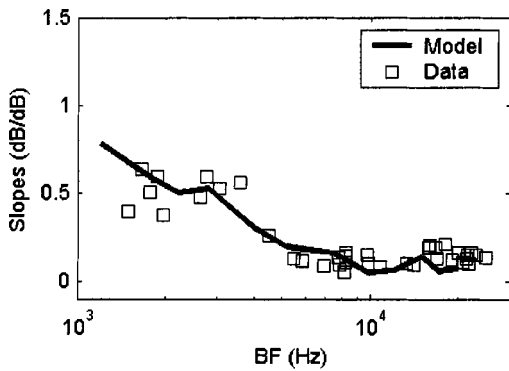
FIG. 6. The variation with BF of the slopes of derived input–output functions at high intensities. Squares are data from the guinea-pig (Cooper and Yates, 1994); continuous line is the model data.

now spreads to lower frequencies at high levels. Figures 7(c) and (d) (reproduced from Müller and Robertson 1991, Fig. 7) show the responses of two fibers from around 9-kHz BF in a single animal, having low- and high-SR fibers, respectively. At high BFs, the response has a pronounced tip, with the activity spreading clearly downwards at high levels. Figures 7(e)–(h) show the response of the model to these stimuli. The DRNL filter stage used the filterbank parameters of Table I, and the IHC parameters were manipulated as in Sec. III B. The parameter values are given in the figure legend. The model reproduces most of the effects observed in the data, including the shift of BF with level. In the model, the direction of the shift with BF depends on the relative center frequencies of the linear and nonlinear DRNL filter pathways. As the level rises, the BF shifts towards the center frequency of the linear path. At high BFs the response shifts

down to lower frequencies as level rises. At BFs below 1 kHz the response shifts up to higher frequencies as the level increases. This general trend is also consistent with the directions of frequency glides in cat AN impulse responses (Carney et al., 1999).

D. RI characteristics for different fiber types

AN fiber rate-responses differ within a given BF range as well as along the length of the cochlea (Yates et al., 1990; Sachs and Abbas, 1974). Here we are particularly interested in how RI shape varies with BF. In the guinea-pig, the basic three shapes are found across most of the BF range (Winter et al., 1990). However, Winter and Palmer (1991) report finding no straight RI functions below 1.5 kHz. No straight RI functions have ever been reported in the cat.

Figure 8 shows RI responses from the filterbank for the three different generic IHC settings in Table I, both for stimulus frequencies at BF (continuous lines) and one octave below (dashed lines). The three models differ only in the values of IHC parameters G_{Ca}^{max} and $[Ca^{2+}]_{thr}$. G_{Ca}^{max} decreases and $[Ca^{2+}]_{thr}$ increases as SR decreases. These values are the same at all BFs. Each fiber type shows the correct characteristic RI function at BF. The responses to stimuli an octave below BF do not show compression. As low as 3 kHz, the LSR RI functions are of the straight type. Below this, only saturating and sloping-saturation RI functions exist. The RI functions at 12-kHz BF [Figs. 8(b) and (c)] are non-monotonic, and actually fall at levels above 90 dB. The outputs from the two filter pathways are out of phase and cancel each other out. Such features have been observed in the auditory nerve fibers of cats, and are associated with a 180°
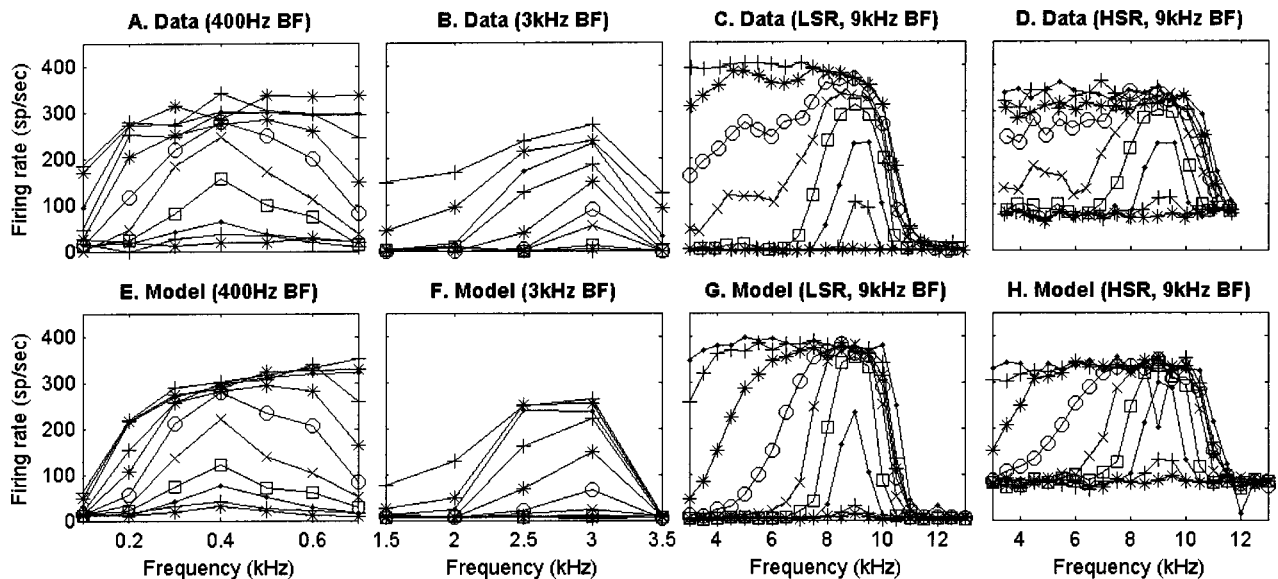

FIG. 7. Iso-intensity rate-responses of guinea-pig AN fibers and the model, for various BFs and SRs. (a)–(d). Guinea-pig AN responses provided by Winter and Robertson (a, b) and reproduced from Müller and Robertson (1991) (c, d). (e)–(h) Model AN fiber responses to the same stimuli and BFs as (a)–(d). All use the DRNL filterbank parameter set (Table I), with IHC parameters and middle ear gain varied to obtain best fit as described in text. (a) Guinea-pig AN fiber with a BF of 400 Hz. Each connected set of symbols has a constant stimulus level, ranging from 35 to 85 dB SPL in 5-dB increments. (b) Guinea-pig AN fiber with a BF of 3 kHz. Stimulus levels range from 41 to 91 dB SPL in 5-dB increments. (c) Low-SR guinea-pig AN fiber with a BF of 9 kHz. Stimulus levels range from 30 to 100 dB SPL in 10-dB increments. (d) High-SR guinea-pig AN fiber with a BF of 9 kHz. Stimulus levels range from 20 to 100 dB SPL in 10-dB increments. (e) Model with a BF of 400 Hz and $G_{Ca}^{max}=8.3$ nS, $[Ca^{2+}]_{thr}=5\times10^{-11}$, $M=12$, and $G_{me}=0$. (f) Model with a BF of 2820 Hz and $G_{Ca}^{max}=2.7$ nS, $[Ca^{2+}]_{thr}=1.2\times10^{-11}$, $M=14$, and $G_{me}=-30$ dB. (g) LSR model with a BF of 9 kHz and $G_{Ca}^{max}=5$ nS, $[Ca^{2+}]_{thr}=3\times10^{-11}$, $M=14$, and $G_{me}=-10$ dB. (h) HSR model with a BF of 9 kHz and $G_{Ca}^{max}=8.5$ nS, $[Ca^{2+}]_{thr}=4.48\times10^{-11}$, $M=12$, and $G_{me}=-10$ dB.
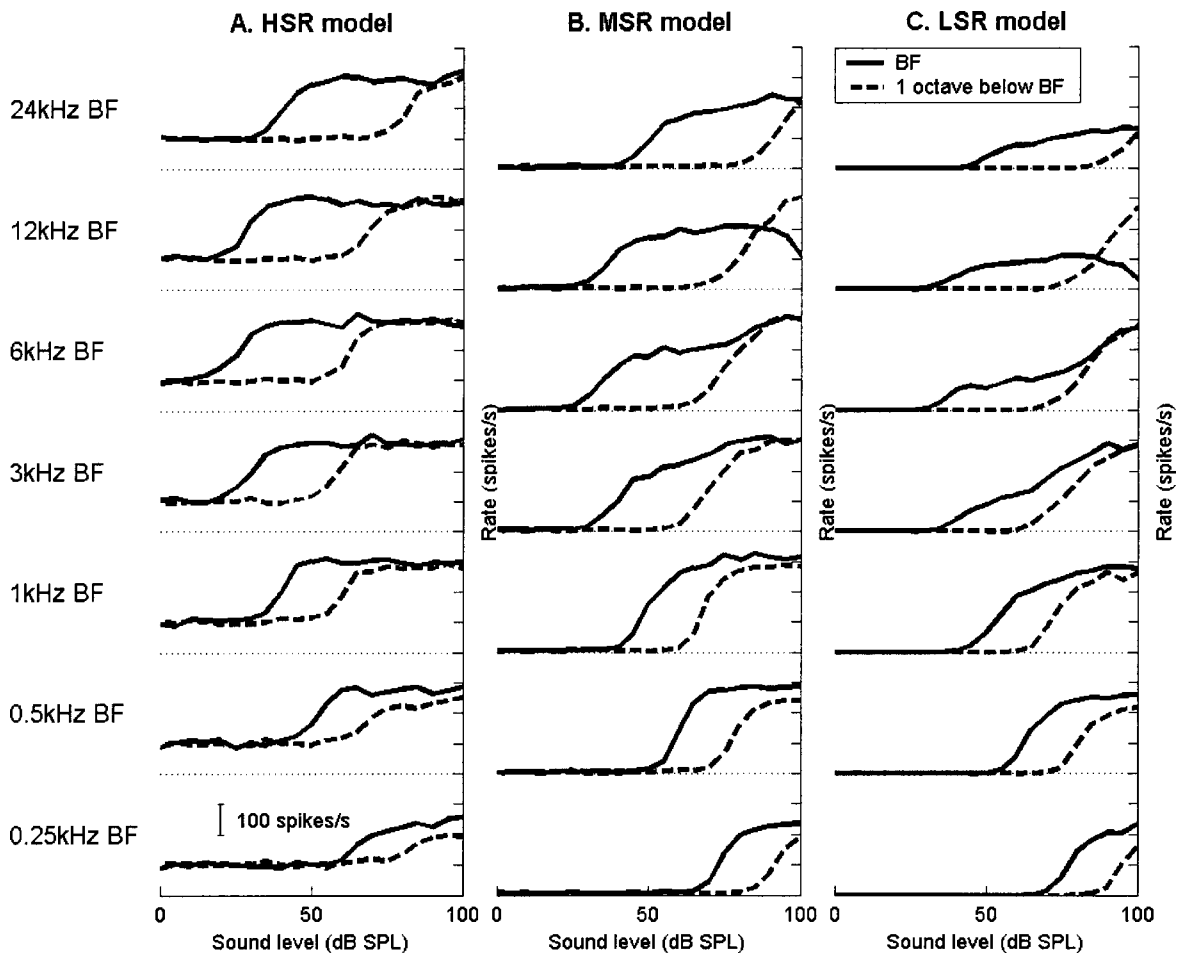
FIG. 8. RI functions from across the filter-bank for (a) high, (b) medium, and (c) low-spontaneous rate fiber types. Continuous lines are the responses at BF (indicated to the left of the panels) and dashed lines are the response for the same filter-bank channel, stimulated at one octave below its BF. All responses use the DRNL filterbank, and the synapse parameters are the "HSR," "MSR," and "LSR" parameter sets given in Table I.

phase shift in the period histograms (e.g., Liberman and Kiang, 1984).

Figure 9 shows how the threshold and spontaneous rate vary with G_{Ca}^{max}. Figure 9(a) shows how the threshold varies with SR in the model, for BF stimulation at two different frequencies (solid lines). The threshold is calculated from rate-level functions as the point at which the rate is 20 spikes/s above the spontaneous rate. The threshold first drops steeply, and then more slowly as the spontaneous rate grows. This trend is compared with the data of Winter and Palmer (1991; dots). In order to satisfy the multiple constraints of SR, threshold, and the shape of the RI function, it was necessary to co-vary $[Ca^{2+}]_{thr}$ with G_{Ca}^{max}:

$$[Ca^{2+}]_{thr} = \frac{4.5 \times 10^{-11}}{[1 + e^{8 \times 10^9 (G_{Ca}^{max} - 1.5 \times 10^{-9})}]}. \quad (4)$$

The model threshold does not appear to change at low SRs. Due to the calcium threshold, at low values of G_{Ca}^{max} the SR becomes zero. However, the threshold continues to shift. Figure 9(b) shows how spontaneous rate varies with the maximum-calcium-conductance parameter, G_{Ca}^{max}. $[Ca^{2+}]_{thr}$ is set according to Eq. (4). The continuous line shows the theoretical values calculated from Eq. (3). The single points indicate the values calculated from the model outputs.

IV. DISCUSSION

We have presented a nonlinear filterbank fitted, as far as possible, to guinea-pig AN data for threshold tuning curves, RI functions and compressive nonlinearities. The model is adequate to provide useful responses to pure tones, across a wide range of BFs and stimulus frequencies. It should prove useful as an input to models of more central processes that require nonlinear cochlear properties that vary appropriately with BF. It is especially suited for studying level dependent rate effects, differences between different fiber types, and differences in AN rate responses along the cochlear partition.

There are many response characteristics that have not been considered here. We have restricted the study to rate responses only. Other characteristics of the DRNL filter and IHC models have been considered individually elsewhere (Meddis et al., 2001; Sumner et al., 2002, 2003). These include tuning and nonlinearity at the level of the BM, local distortion products, impulse responses, phase locking, discharge history effects, adaptation, and the variation of pure tone PSTHs with fiber type.

In order to simplify the implementation, the compression exponent and filter orders were fixed across all BFs. It is especially interesting that the same highly compressive exponent value of 0.1 dB/dB could be used at all BFs. The
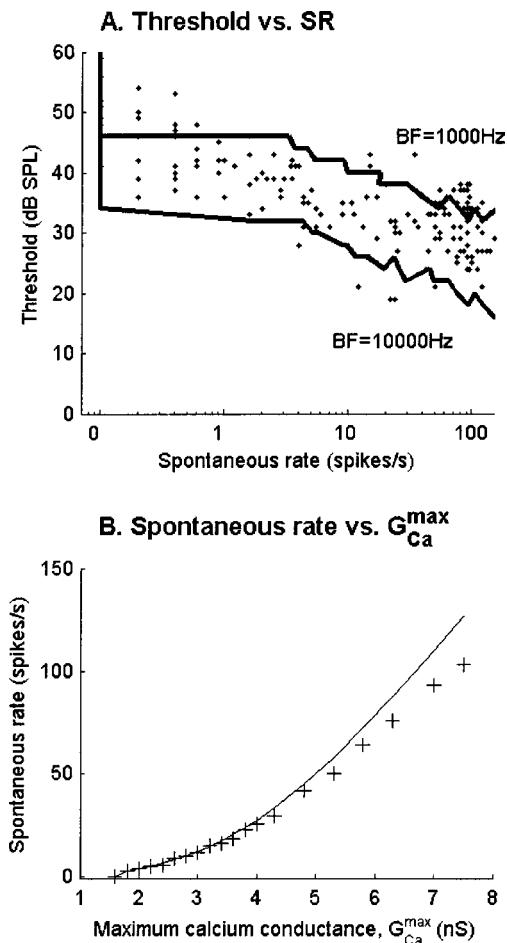
A. Threshold vs. SR

B. Spontaneous rate vs. G_{Ca}^{max}

FIG. 9. (a) The relationship between threshold and SR. The solid line show the response of the model for BF stimulation at two different frequencies lines. The dots show the data of Winter and Palmer (1991). Threshold in the model is defined as the point at which the rate reaches $20 \ s^{-1}$ above the spontaneous firing rate. (b) The relationship between SR and G_{Ca}^{max}. $[Ca^{2+}]_{thr}$ co-varies with G_{Ca}^{max} as described in the text. The continuous line shows the value predicted by Eq. (3). Crosses show the value calculated at the output of the AN model.

regions with a derived IO slope of greater than 0.1 arise because at lower BFs the I/O slope is a function of the output of both linear and nonlinear pathways. Thus a functional variation in compression emerges from changes in the relative contributions of the pathways at BF. Below 1 kHz the BF IO function of the model is mostly linear. However, distortion products are still produced by the nonlinear pathway and are thus present in its response. The variation in measured nonlinearity could have been achieved by varying the compression exponent, ν, with BF. However, we sought to vary the smallest number of parameters possible, and it was not necessary to vary ν here. The filter orders were fixed across the whole filterbank, and this has compromised the fit of the model in some cases. The logarithmic function of linear path gain with BF was another limitation. A better fit to all BFs would have been possible with a more complicated scheme. However, we felt that this could not be justified without a larger data set.

The IO function of the mechanical filtering was assumed to be linear for stimulation frequencies well below BF. This is supported by BM laser interferometry results (Ruggero

et al., 1997; Nuttall and Dolan, 1996) at high BFs. At very low BFs ($\sim$250 Hz), BM IO functions are mostly linear at all stimulus frequencies (Cooper and Rhode, 1995). However, what nonlinearity there is seems to extend across a wide range of frequencies. If the BM is compressed at the below-BF stimulus frequency, the resulting derived IO function for the BF response will be less compressed than the underlying mechanical input. At BFs in the range of 1–5 kHz, there are no direct BM measurements. Therefore it is difficult to assess the validity of the assumption here. The shapes of AN FTCs change rapidly with BF when the fiber BFs are below a few kilohertz. It seems probable that IO functions are also varied. We can only comment that the response of the model presented here is linear at 700 Hz for a BF of 1800 Hz and fits the RI functions quite well [Fig. 5(d)]. Therefore it seems to be a reasonable assumption in this instance.

ACKNOWLEDGMENTS

[1]The software is available in two forms. DSAM (development system for auditory modelling) is a C library containing an extensive collection of auditory model components, and support routines. AMS (auditory model simulator) is a cross-platform application, providing a flexible GUI interface for all the models supported by DSAM. These can be downloaded from www.essex.ac.uk/psychology/hearinglab/dsam, together with the simulation scripts required to configure the model correctly.

Assman, P., and Summerfield, Q. (**1990**). "Modelling the perception of concurrent vowels: Vowels with different fundamental frequencies," J. Acoust. Soc. Am. **85**, 327–338.

Brandenburg, K. (**1996**). "Introduction to Perceptual Coding," in *Collected Papers on Digital Audio Bit-Rate Reduction*, edited by N. Gilchrist and C. Grewin, Audio Eng. Soc. ISBN 0-937803-33-2.

Brandenburg, K., and Bosi, M. (**1997**). "Overview of MPEG Audio: Current and Future Standards for Low-Bit-Rate Audio Coding," J. Audio Eng. Soc. **45**, 4–21.

Brown, G. J., and Cooke, M. (**1994**). "Computational auditory scene analysis," Comput. Speech Lang. **8**, 297–336.

Carney, L. H. (**1993**). "A model for the responses of low-frequency auditory-nerve fibers in cat," J. Acoust. Soc. Am. **93**, 401–417.

Carney, L. H., McDuffy, M. J., and Shekhter, I. (**1999**). "Frequency glides in the impulse response of auditory nerve-fibers," J. Acoust. Soc. Am. **105**, 2384–2391.

Cooper, N. P., and Rhode, W. S. (**1995**). "Nonlinear mechanics at the apex of the guinea-pig cochlea," Hear. Res. **82**, 225–243.

Cooper, N. P., and Yates, G. K. (**1994**). "Non-linear input-output functions derived from the responses of guinea-pig cochlear nerve fibres: Variations with characteristic frequency," Hear. Res. **78**, 221–234.

Deng, L., and Geisler, C. D. (**1987**). "A composite model for processing speech sounds," J. Acoust. Soc. Am. **82**, 2001–2012.

Ellis, D. P. W. (**1996**). "Prediction-driven computational auditory scene analysis," Ph.D. Thesis, MIT.

Evans, E. F. (**1972**). "The frequency response and other properties of single fibers in the guinea-pig cochlear nerve," J. Physiol. (London) **226**, 263–287.

Ghitza, O. (**1988**). "Temporal non-place information in the auditory-nerve firing patterns as a front-end for speech recognition in a noisy environment," J. Phonetics **16**, 109–123.

Giguere, C., and Smoorenburg, G. F. (**1998**). "Computational modeling of outer hair cell damage: implications for hearing and signal processing," in *Psychophysics, Physiology and Models of Hearing* (World Scientific, Singapore), pp. 155–164.

Giguere, C., and Woodland, P. C. (**1994**). "A computational model of the auditory periphery for speech and hearing research I. Ascending path," J. Acoust. Soc. Am. **95**, 331–342.

Goldstein, J. L. (**1990**). "Modeling rapid waveform compression on the basilar membrane as multiple-bandpass-nonlinearity filtering," Hear. Res. **49**, 39–60.

Goldstein, J. L. (**1995**). "Relations amount compression, suppression and combination tones in mechanical responses of the basilar membrane: data and MBPNL model," Hear. Res. **89**, 52–68.

Hartung, K., and Trahiotis, C. (**2001**). "Peripheral auditory processing and investigations of the "precedence effect" which utilize successive transient stimuli," J. Acoust. Soc. Am. **110**, 1505–1513.

Hermansky, H. (**1998**). "Should recognizers have ears?" Speech Commun. **25**, 3–24.

Hewitt, M. J., and Meddis, R. (**1992**). "Regularity of cochlear nucleus stellate cells: A computational modeling study," J. Acoust. Soc. Am. **93**, 3390–3399.

Irino, T., and Patterson, R. D. (**2001**). "A compressive gammachirp auditory filter for both physiological and psychological data," J. Acoust. Soc. Am. **109**, 2008–2022.

Jenison, R. L., Greenberg, S., Kleunder, K. R., and Rhode, W. S. (**1991**). "A composite model of the auditory periphery for the processing of speech based on the filter functions of single auditory-nerve fibers," J. Acoust. Soc. Am. **90**, 773–785.

Liberman, M. C., and Kiang, N. Y. S. (**1984**). "Single-neuron labeling and chronic cochlear pathology. IV. Stereocilia damage and alterations in rate- and phase level-functions," Hear. Res. **16**, 75–90.

Lopez-Poveda, E. A., and Meddis, R. (**2001a**). "A human nonlinear cochlear filterbank," J. Acoust. Soc. Am. **110**, 3107–3118.

Lopez-Poveda, E. A., and Meddis, R. (**2001b**). "A human nonlinear cochlear filterbank," #827, ARO Midwinter research meeting, Florida.

Meddis, R. (**1986**). "Simulation of mechanical to neural transduction in the auditory receptor," J. Acoust. Soc. Am. **79**, 702–711.

Meddis, R. (**1988**). "Simulation of auditory-neural transduction: Further studies," J. Acoust. Soc. Am. **83**, 1056–1063.

Meddis, R., and Hewitt, M. J. (**1991a**). "Virtual pitch and phase sensitivity of a computer model of the auditory periphery. I. Pitch Identification," J. Acoust. Soc. Am. **89**, 2866–2882.

Meddis, R., and Hewitt, M. J. (**1991b**). "Virtual pitch and phase sensitivity of a computer model of the auditory periphery. II. Phase sensitivity," J. Acoust. Soc. Am. **89**, 2883–2894.

Meddis, R., and Hewitt, M. J. (**1992**). "Modeling the identification of concurrent vowels with different fundamental frequencies," J. Acoust. Soc. Am. **91**, 233–245.

Meddis, R., O'Mard, L. P., and Lopez-Poveda, E. A. (**2001**). "A computational algorithm for computing nonlinear auditory frequency selectivity," J. Acoust. Soc. Am. **109**, 2852–2861.

Müller, M., and Robertson, D. (**1991**). "Relationship between tone burst discharge pattern and spontaneous firing rate of auditory nerve fibers in the guinea-pig," Hear. Res. **57**, 63–70.

Nuttall, A. L., and Dolan, D. F. (**1996**). "Steady-state sinusoidal velocity responses of the basilar membrane in guinea-pig," J. Acoust. Soc. Am. **99**, 1556–1565.

Patterson, R. D., Allerhand, M. H., and Giguére, C. (**1995**). "Time domain modeling of peripheral auditory processing: A modular architecture and a software platform," J. Acoust. Soc. Am. **98**, 1890–1894.

Patterson, R. D., Nimmo-Smith, I., Holdsworth, J., and Rice, P. (**1988**). "Spiral vos final report, Part A: The auditory filterbank," Cambridge Electronic Design, Contract Rep. (Apu 2341).

Pressnitzer, D., Cheveigne, A., and Winter, I. M. (**2002**). "Perceptual pitch shift for sounds with similar waveform autocorrelation," Acoustic Research Letters On-line **3**(1).

Relkin, E. M., and Pelli, D. G. (**1987**). "Probe tone thresholds in the auditory-nerve measured by 2-interval forced choice procedures," J. Acoust. Soc. Am. **82**, 1679–1691.

Rhode, W. S. (**1971**). "Observations for vibration of the basilar membrane using the Mossbauer technique," J. Acoust. Soc. Am. **49**, 1218–1231.

Robert, A., and Eriksson, J. L. (**1999**). "A composite model of the auditory periphery for simulating responses to complex sounds," J. Acoust. Soc. Am. **106**, 1852–1864.

Ruggero, M., Rich, N. C., Recio, A., Narayan, S. S., and Robles, N. (**1997**). "Basilar membrane responses to tones at the base of the chinchilla," J. Acoust. Soc. Am. **101**, 2151–2163.

Sachs, M. B., and Abbas, P. J. (**1974**). "Rate versus level functions for auditory-nerve fibers in cats: tone burst stimuli," J. Acoust. Soc. Am. **56**, 1835–1847.

Sachs, M. B., Bruce, I. C., Miller, R. L., and Young, E. D. (**2002**). "Biological basis of hearing aid design," Ann. Biomed. Eng. **30**, 157–168.

Schoonhoven, R., Keijzer, J., Versnel, H., and Prijs, V. F. (**1994**). "A dual filter model describing single-fiber responses to clicks in the normal and noise-damaged cochlea," J. Acoust. Soc. Am. **95**, 2104–2121.

Shamma, S. A., Chadwick, R. S., Wilbur, W. J., Morrish, K. A., and Rinzel, J. (**1986**). "A biophysical model of the cochlear processing: Intensity dependence of pure tone responses," J. Acoust. Soc. Am. **80**, 133–145.

Summer, C. J., Lopez-Poveda, E. A., O'Mard, L. P., and Meddis, R. (**2002**). "A revised model of the inner-hair-cell and auditory nerve complex," J. Acoust. Soc. Am. **111**, 2178–2188.

Sumner, C. J., Lopez-Poveda, E. A., O'Mard, L. P., and Meddis, R. (**2003**). "Adaptation in a revised inner-hair cell model," J. Acoust. Soc. Am. **113**, 893–901.

Tchorz, J., and Kollmeier, B. (**1999**). "A model of auditory perception as a front end for automatic speech recognition," J. Acoust. Soc. Am. **106**, 2040–2050.

Winter, I. M., and Palmer, A. R. (**1991**). "Intensity coding in low-frequency auditory-nerve fibers of the guinea-pig," J. Acoust. Soc. Am. **90**, 1958–1967.

Winter, I. M., Robertson, D., and Yates, G. K. (**1990**). "Diversity of characteristic frequency rate-intensity functions in guinea pig auditory nerve fibers," Hear. Res. **45**, 191–202.

Yates, G. K., Winter, I. M., and Robertson, D. (**1990**). "Basilar membrane nonlinearity determines auditory nerve rate-intensity functions and cochlear dynamic range," Hear. Res. **45**, 203–220.

Zhang, X. D., Heinz, M. G., Bruce, I. C., and Carney, L. H. (**2001**). "A phenomenological model for the responses of auditory-nerve fibers: I. Non-linear tuning with compression and suppression," J. Acoust. Soc. Am. **109**, 648–670.